Diagn Interv Radiol 2012; 18:391–396

ORIGINAL ARTICLE

Imaging features of bone metastases in patients with gastrointestinal stromal tumors

Anupma Jati, Servet Tatlı, Jeffrey A. Morgan, Jonathan N. Glickman, George D. Demetri, Annick Van den Abbele, Stuart G. Silverman

PURPOSE
To determine the prevalence and imaging features of bone metastases in patients with gastrointestinal stromal tumors (GISTs).

MATERIALS AND METHODS
The medical records of 190 patients with pathologically proven GISTs were reviewed, and patients with bone metastases were identified. Computed tomography (CT) scans of the chest, abdomen, and pelvis were examined for features of bone metastases, and findings were correlated with the results of positron-emission tomography (PET) and histopathology.

RESULTS
Of 190 GIST patients, six (3.2%) had bone metastases: four patients had multiple bone metastases, and two patients had a solitary metastasis. The maximum diameter of the metastases ranged from 2 to 40 mm, and they most commonly involved the vertebrae, ribs, pelvic bones, and femurs. All lesions were well-marginated and lytic. A soft tissue component was identified in three patients. The bone metastases showed intense fluorine-18 fluorodeoxyglucose (FDG) uptake. After treatment with imatinib mesylate in three patients, the bone metastases developed peripheral sclerosis on CT and became less FDG-avid on PET. All six primary tumors were morphologically high-grade with high mitotic rates and necrosis.

CONCLUSION
Bone metastases from GISTs are uncommon; when detected with CT, they are characterized by single or multiple lytic lesions with or without soft tissue involvement. A sclerotic rim may appear around the metastatic lesions in response to treatment. Similar to the disease in other sites, bone metastases show intense FDG uptake, which decreases following treatment.

Key words: • *gastrointestinal stromal tumors* • *metastases* • *bone* • *positron-emission tomography and computed tomography*

From the Departments of Radiology (A.J., A.V.A.) and Oncology (J.A.M., G.D.D.), Harvard Medical School, Dana Farber Cancer Institute, Boston, Massachusetts, USA; the Departments of Radiology (S.T. ✉ *statli@partners.org*, S.G.S.) and Pathology (J.N.G.), Harvard Medical School, Brigham and Women's Hospital, Boston, Massachusetts, USA.

Received 27 September 2011; revision requested 18 October 2011; revision received 19 October 2011; accepted 24 October 2011.

Published online 9 March 2012
DOI 10.4261/1305-3825.DIR.5179-11.1

Gastrointestinal stromal tumors (GISTs) are rare mesenchymal tumors of the gastrointestinal tract, accounting for 1%–3% of all malignant gastrointestinal tumors (1–5). Most GISTs are benign; malignant tumors account for 20%–30% of cases (1). GISTs arise most commonly from the stomach (60%), followed by the small intestine (25%), rectum (5%), and other locations in the gastrointestinal tract (1, 2). Tumors arising outside the gastrointestinal tract, such as in the mesentery or omentum, constitute up to 10% of cases (4). The liver is the most common site of metastatic disease (5). GISTs can metastasize to many other organs, including the omentum and mesentery. Lymph node involvement and lung metastases are rare (4–6). Bone metastases have been reported, but their true prevalence is unknown (6, 7). It is important to recognize bone metastases since they may subsequently develop skeletal-related events associated with severe morbidity.

To our knowledge, there is no published description of the imaging features of bone metastases in patients with GISTs. Therefore, we evaluated the prevalence and imaging features of bone metastases in patients with malignant GISTs.

Materials and methods

Subjects

Approval was obtained from our Institutional Review Board to review the medical records and imaging studies of 190 patients with pathologically proven GIST, who were enrolled in the tyrosine kinase inhibitor (imatinib mesylate, Gleevec, Novartis Pharmaceuticals, East Hanover, New Jersey, USA) trial between May 2000 and September 2005. One radiologist reviewed the database retrospectively and identified six (3.2%) patients with metastatic bone lesions. The metastases were proven by either fluorine-18 fluorodeoxyglucose (FDG) positron-emission tomography (PET) activity (n=4) or histopathology obtained from a percutaneous biopsy (n=2) (Table 1). Five patients were men, and the mean patient age was 55 years (range, 48–71 years). The diagnosis of GIST was established either by surgical resection (n=5) or biopsy (n=1) of the primary tumor. All primary tumors were larger than 6 cm (mean, 10.5 cm; range, 6–18.5 cm) at the time of resection or diagnosis. The primary sites of the GIST were the stomach (n=4), rectum (n=1), and jejunum (n=1). In addition to bone, patients had metastases in the liver (n=6), peritoneum/mesentery (n=5), spleen (n=1), lymph nodes (n=1), and soft tissues (n=2). In all six patients with bone metastases, a diagnosis of metastatic GIST was made by liver biopsy.

The mean time interval from the initial presentation of GIST to the detection of bone metastases was three years (range, 3 months–6 years). The patients either had bone metastases (n=5) before starting tyrosine kinase inhibitor therapy or developed bone metastases (n=1) while being

Table 1. Demographics and histopathology of six patients with gastrointestinal stromal tumors and bone metastases

Patient	Age (years)	Gender	Location[a]	c-kit protein	Mitosis/HPF	Necrosis	Metastases[b]
1	49	Male	Stomach	+	27/50	+	L, S, P, LN, ST
2	71	Male	Rectum	+	41/50	+	L, P
3	52	Female	Stomach	+	40/50	-	L, P
4	48	Male	Stomach	+	12/50	+	L, P
5	51	Male	Stomach	+	22/50	+	L, P, ST
6	60	Male	Jejunum	+	6/50	+	L

HPF, high-power field.
[a]Location of the primary site.
[b]Sites of metastases: liver (L), peritoneum (P), spleen (S), soft tissue (ST), lymph node (LN).

treated. None of the patients had other malignant tumors.

Pathologic examination and analysis

For each of the six patients with bone metastases, pathology slides from the primary tumor (n=6), liver biopsy specimens (n=6), and bone metastases (n=2) were reviewed and the diagnosis of GIST was confirmed. In addition, immunohistochemical staining for c-kit protein, CD-34, and other smooth muscle markers (desmin and actin) was performed, and the tumor grades were recorded.

Imaging technique and analysis

All patients had contrast-enhanced chest, abdomen, and pelvis computed tomography (CT), which was performed using a multidetector scanner (Volume Zoom, Siemens Medical Solutions, Forchheim, Germany) with a section thickness of 5–7 mm, after administering 100 mL of nonionic intravenous contrast (Ultravist 300, Schering, Germany). Within 1–3 days of the CT, three patients underwent whole-body (from the skull base to the upper thighs) PET (ECAT Exact HR+, Siemens/CTI, Knoxville, Tennessee, USA) and one underwent PET-CT (Discovery LS, GE Medical Systems, Milwaukee, Wisconsin, USA) following four hours of fasting, and 18–22 mCi of FDG was administered intravenously with a 45–60 min delay.

A nuclear medicine physician reviewed the PET images and identified abnormal FDG activity in bones and soft tissues. On PET, the bone and liver lesions were evaluated by visual inspection, and the maximum standardized uptake value (SUV_{max}) was calculated as (region of interest counts/injected dose)×body weight using attenuation-corrected images.

Two radiologists reviewed the CT images on picture archiving and communication system monitors and identified the biopsied bone metastases (in two patients) and bone metastases with corresponding FDG uptake on PET scans (in four patients). The following features were recorded: number, location, size, margins, and density (lytic, sclerotic, or mixed) of the metastases; whether they were discrete or confluent; and the presence of an associated extraosseous soft tissue component.

Follow-up chest, abdomen, and pelvic CT (in six patients) and whole-body PET (in four patients) were also reviewed, and any changes from the initial readings were noted. Other available radiology examinations were also reviewed, including spine magnetic resonance imaging (MRI) in one patient and plain radiographs of the chest and abdomen in another.

Results

Imaging analysis

Of 190 GIST patients, six (3.2%) had bone metastases, which were either multiple (n=4) or solitary (n=2). The metastases involved the pelvic bone (n=4; Fig. 1), ribs (n=4; Fig. 2), vertebrae (n=4; Fig. 3), and femur (n=3); and their maximum diameter ranged from 2 to 40 mm (median, 19 mm). All lesions were well-marginated and lytic (Table 2). Except in one patient, all lesions were discrete. There were no sclerotic components in any lesion. In five patients, the metastases caused cortical disruption, which led to fractures in two patients. There was an associated soft tissue component in three patients. In four patients who underwent PET, the bone metastases showed intense FDG uptake (mean SUV_{max}, 8.7; range, 6.7–11), which was similar to that of liver metastases (mean SUV_{max}, 13.4; range 10–20).

In the patient who underwent MRI, the spine metastases were hypointense on T1-weighted images and hyperintense on T2-weighted images. In addition, metastases involved the left pedicle of the L5 vertebra with an enhancing soft tissue component, which was compressing the spinal cord.

After therapy was initiated, the bone lesions showed interval development of peripheral sclerosis on CT in three patients. The plain radiograph in one patient showed multiple well-defined lytic lesions, some with sclerotic margins suggesting a treatment response. On follow-up PET obtained after treatment, the lesions showed decreased FDG avidity in three patients (mean SUV, 2.8; range, 2.0–4.1) paralleling that of the liver metastases (mean SUV, 3.3; range, 2.1–5.0), suggesting a treatment response (Table 2). In one patient, both the bone and liver metastases progressed; the bone lesions were more FDG-avid and no peripheral sclerosis developed on CT.

Correlation with pathology and immunohistochemical analyses

All six primary tumors were of high-grade morphologically with high mitotic rates (6–41 per 50 high power fields) and necrosis.

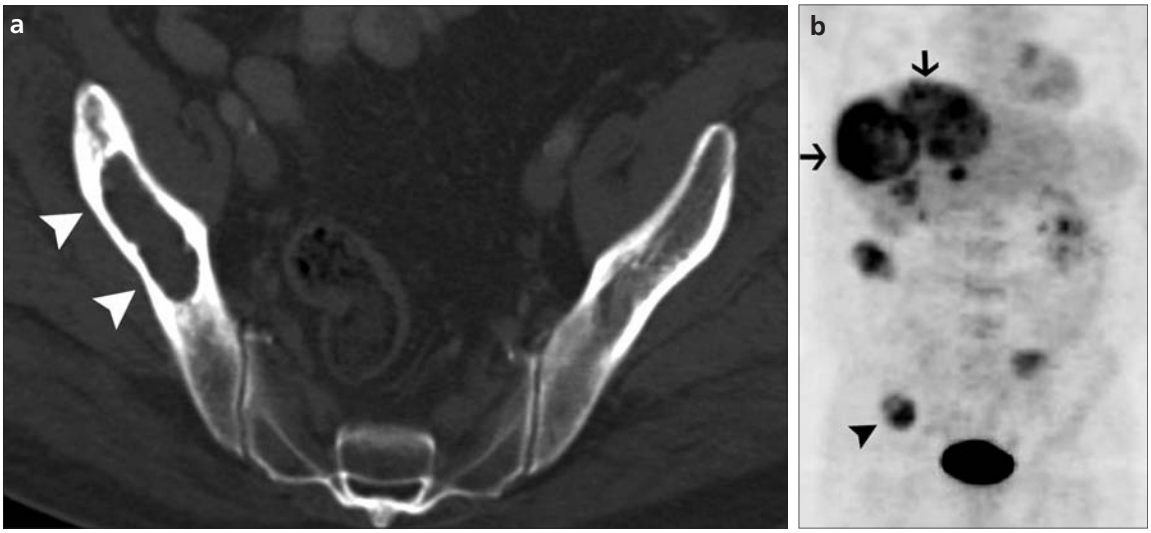

Figure 1. a, b. A 60-year-old man with GIST of the jejunum. Axial contrast-enhanced CT **(a)** shows a single well-marginated metastatic lytic lesion in the right iliac bone *(arrowheads)*. Although the CT appearance is not typical for a metastasis, the coronal PET image **(b)** shows that the lytic lesion in the right iliac bone is FDG-avid and consistent with metastasis *(arrowhead)*. Note also the FDG-avid liver metastases **(b,** *arrows***)**.

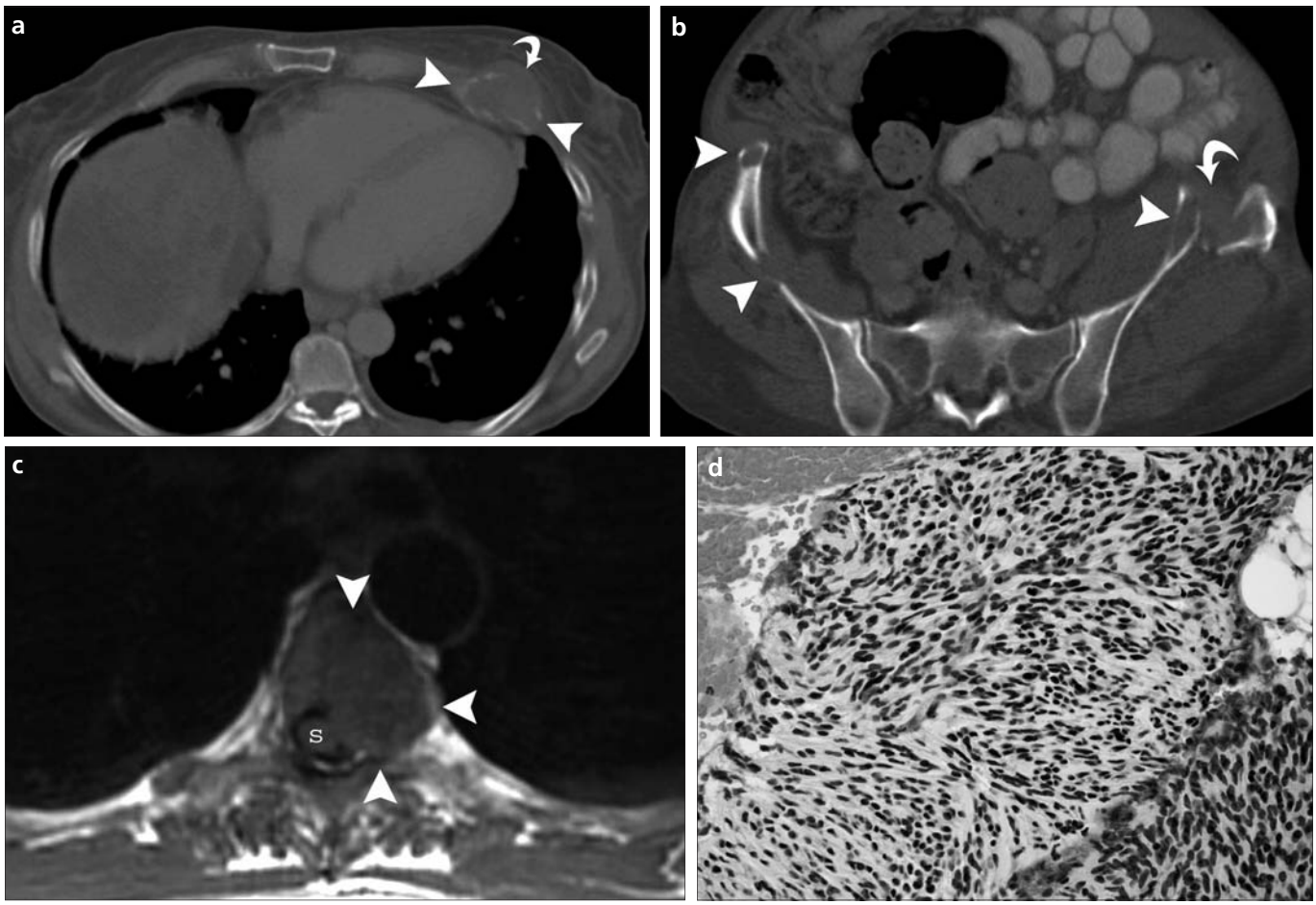

Figure 2. a–d. A 52-year-old woman with GIST of the stomach. Axial contrast-enhanced CT at the level of the lung bases **(a)** shows a lytic lesion involving the left anterior 8th rib *(arrowheads)* with a soft tissue component *(curved arrow)*. Axial contrast-enhanced CT at the level of the pelvis **(b)** shows multiple lytic lesions (*arrowheads*), one of which has caused a displaced fracture of the left iliac bone *(curved arrow)*. Axial T1-weighted MRI at the level of the lower thoracic spine **(c)** shows an intermediate signal intensity mass *(arrowheads)* involving the left pedicle and corpus of the vertebral body, extending into the spinal canal, and compressing the spinal cord. Photomicrograph of the biopsy specimen of the left rib lesion **(d)** shows a hypercellular spindle-cell neoplasm consistent with metastatic GIST (hemotoxylin-eosin, ×400).

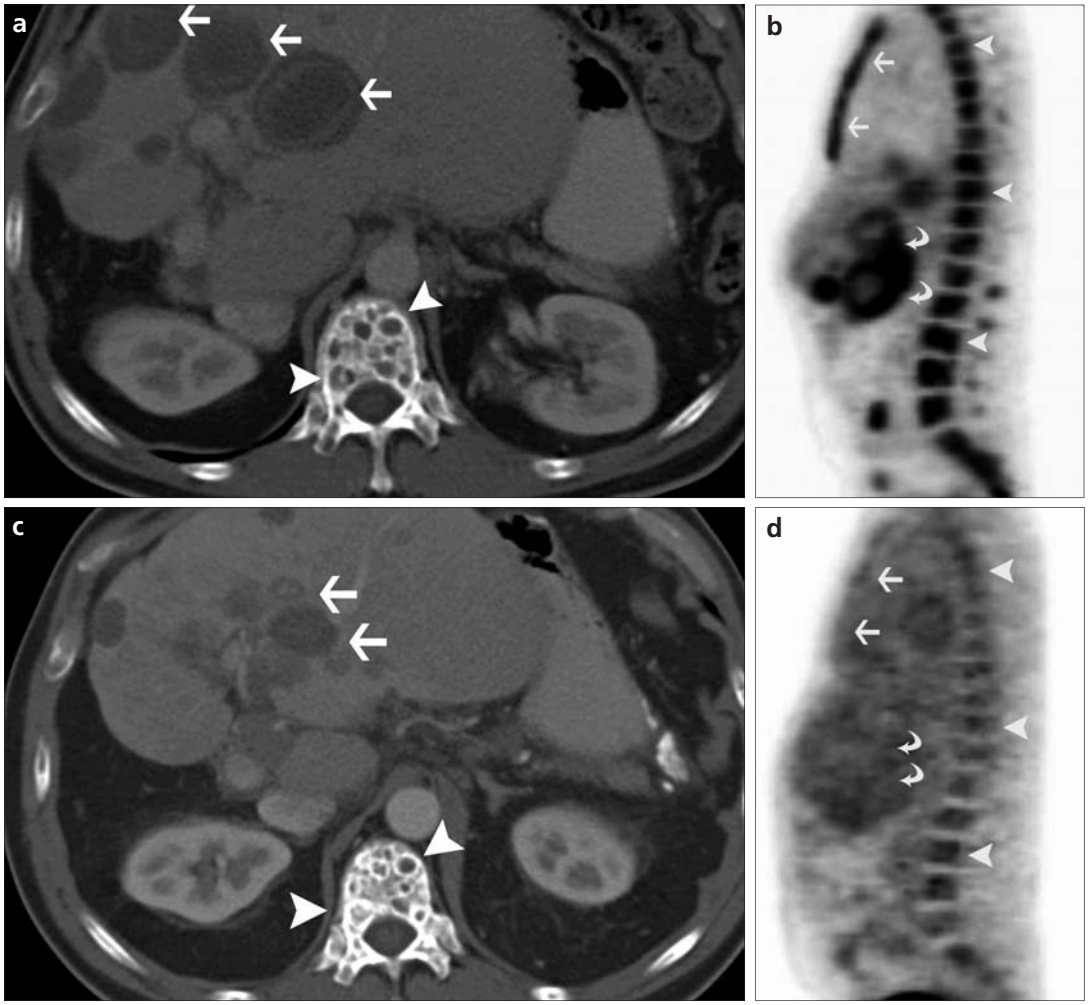

Figure 3. a–d. A 49-year-old man with GIST of the stomach. Axial contrast-enhanced CT image at the level of the liver **(a)** shows multiple well-marginated lytic lesions *(arrowheads)* throughout the lower thoracic vertebra. Note multiple low attenuating masses *(arrows)* in the liver. Sagittal PET **(b)** shows that masses in the spine *(arrowheads)* and sternum *(arrows)* are markedly FDG-avid, as are the liver masses, which are consistent with metastases *(curved arrows)*. Axial contrast-enhanced CT **(c)** obtained following the completion of imatinib mesylate therapy shows that a sclerotic rim is developed around the lytic lesions in the vertebra *(arrowheads)*. Note that the liver lesions are smaller and less prominent *(arrows)* compared to the pretreatment CT in Fig. 3a. Sagittal PET image (**d**) obtained following the completion of imatinib mesylate therapy also shows that the spine *(arrowheads)*, sternum *(arrows)*, and liver *(curved arrows)* masses are less FDG-avid.

Table 2. CT and PET imaging findings of bone metastases in six patients with gastrointestinal stromal tumors

	Initial CT/PET									Follow-up CT/PET		
Patients	Number	Location	Size (cm)	Margin	Density	D vs. C	EOS	Bone (SUV_{max})	Liver (SUV_{max})	Sclerosis	Bone (SUV_{max})	Liver (SUV_{max})
1	M	V, R, P, F, H	0.2–1.5	W	Lytic	D, C	N	7. 2	10.7	Sclerotic margins	2.4	2. 1
2	M	V, R, P, F, H,	0.4 –4.0	W	Lytic	D	Y	10.0	13.0	No sclerosis	11.3	14.5
3	M	V, R, P	0.9–3.6	W	Lytic	D	Y	N/A	N/A	No sclerosis	N/A	N/A
4	S	V	3.0	W	Lytic	D	Y	11.0	20.0	Sclerotic margins	4.1	5.0
5	M	R, F	0.5–3.0	W	Lytic	D	N	N/A	N/A	Sclerotic margins	N/A	N/A
6	S	P	4.0	W	Lytic	D	N	6.7	10.0	No sclerosis	2.0	2.9

CT/PET, computed tomography/positron-emission tomography; S, single; M, multiple; V, vertebra; R, rib; P, pelvis; F, femur; H, humerus; W, well-defined; D, discrete; C, confluent; EOS, extraosseous soft tissue; Y, yes; N, no; SUV, standardized uptake value; N/A, not available.

Discussion

GISTs are mesenchymal tumors of the gastrointestinal tract with distinct morphologic features that separate them from other smooth muscle and neural tumors. The histopathological diagnosis of GIST in most cases depends on demonstrating the overexpression of c-kit protein (CD117), a tyrosine kinase growth factor receptor, by immunohistochemical staining (8). In fact, targeting this receptor with a c-kit tyrosine kinase inhibitor is of clinical utility in treating patients with unresectable or metastatic GIST, reducing the tumor burden and improving survival (9, 10). Predicting the biological behavior of GIST at the initial diagnosis may be difficult. However, large (>5 cm) tumors, high mitotic activity (>5 mitoses per high-power field), high cellularity, the presence of necrosis, prominent nuclear pleomorphism, and certain activating c-kit mutations are associated with malignant behavior (2).

The traditional initial therapy for patients with GIST has been surgical resection of the primary tumor; however, malignant GISTs typically recur and metastasize (10, 11). The distribution of metastases is generally predictable. The liver is the most common site of metastases at both presentation and relapse (4). The peritoneum is the second most common site of metastases (4, 6), whereas bone metastases are rare (12). Burkill et al. (6) reported bone metastases in two of 83 metastatic disease sites at follow-up in 53 patients with GIST for a frequency of 3.7%, which is similar to our series. However, they did not describe the imaging features of the metastases.

Although bone metastases from GISTs were uncommon in our series, they had a consistent imaging appearance. All bone metastases were lytic and well-defined. The metastatic lesions were often multiple and the axial skeleton was the bone site most commonly involved. Extraosseous soft tissue components were identified in half of the patients. These CT imaging characteristics are not specific to GISTs and are similar to those from other primary tumors. On PET, the bone metastases showed high FDG avidity similar to that of the liver and other sites of metastases. In half of the patients, the bone metastases that responded to treatment developed sclerotic margins on follow-up CT; on PET, the treatment response was correlated with decreased FDG avidity parallel to other sites of metastases. All primary tumors in our series were high-grade and had other sites of metastases.

It is important to identify bone metastases during the imaging surveillance of GIST patients. Bone metastases can cause substantial pain and may also lead to pathological fracture (in two of six patients), hypercalcemia, and spinal cord compression (in one patient) (13, 14). In addition to severe morbidity, skeletal complications may negatively affect the patients' quality of life by impairing mobility and social functioning (13, 14). Since fractures, particularly those involving long bones, have detrimental effects on the patients' quality of life, an effort should be made to predict sites of fracture and preempt their occurrence using systemic and local prophylactic measures (13). Therefore, although rare, the clinician should be aware that bone metastases can occur in patients with metastatic GIST, and any bone lesion in such patients should be evaluated carefully in order to detect and treat bone metastases in a timely manner before serious complications occur.

Depending on the nature of the imminent or actual skeletal complication, a wide variety of treatment options are available to treat bone metastases, including systemic treatment with bisphosphonates, radiation therapy, ablation, vertebroplasty, and surgery (15). Bisphosphonates are potent inhibitors of osteoclast-mediated bone resorption and reduce skeletal complications and provide some pain relief (15).

Our study had limitations. It was a retrospective study, and some patients did not have a histopathological diagnosis of bone metastases. All of these patients had FDG-avid bone lesions with a SUV_{max} similar to that of other site of metastases. Our series included a small number of patients with bone metastases, although bone metastases in patients with GIST are rare. Our patient population consisted of only high-grade tumors. Therefore, the prevalence we found is likely higher than that in a general population of patients with GIST. Regardless of how hard we looked, some bone metastases might have been undetected, which may result in an underestimation of metastasis prevalence.

In conclusion, while rare, lytic bone metastases do occur in patients with high-grade GISTs and most commonly involve the axial skeleton. Bone metastases in GISTs are characterized by single or multiple lytic masses with occasional extraosseous soft tissue involvement, and may develop a sclerotic rim in response to treatment on follow-up CT, like metastases from other primary tumors. In order to identify bone metastases before skeletal complications occur, we recommend evaluating any bone lesions carefully in patients with high-grade GISTs.

Conflict of interest disclosure

The authors declared no conflicts of interest.

References

1. Miettinen M, El-Rifai W, H L Sobin L, Lasota J. Evaluation of malignancy and prognosis of gastrointestinal stromal tumors: a review. Hum Pathol 2002; 33:478–483.
2. Nowain A, Bhakta H, Pais S, Kanel G, Verma S. Gastrointestinal stromal tumors: Clinical profile, pathogenesis, treatment strategies and prognosis. J Gastroenterol Hepatol 2005; 20:818–824.
3. Van der Zwan SM, DeMatteo RP. Gastrointestinal stromal tumor: five years later. Cancer 2005; 104:1781–1788.
4. Dematteo RP, Lewis JJ, Leung D, Mudan SS, Woodruff JM, Brennan MF. Two hundred gastrointestinal tumors: recurrence patterns and prognostic factors for survival. Ann Surg 2000; 231:51–58.
5. Suster S. Gastrointestinal stromal tumors. Semin Diagn Pathol 1996; 13:297–313.
6. Burkill GJ, Badran M, Al-Muderis O, et al. Malignant gastrointestinal stromal tumor: distribution, imaging features, and pattern of metastatic spread. Radiology 2003; 226:527–532.
7. Hersh MR, Choi J, Garrett C, et al. Imaging gastrointestinal stromal tumors. Cancer Control 2004; 12:111–115.
8. Kindblom LG, Remotti HE, Aldenborg F, Meis-Kindblom JM. Gastrointestinal pacemaker cell tumour (GIPACT): gastrointestinal stromal tumors show phenotypic characteristics of the interstitial cells of Cajal. Am J Pathol 1998; 152:1259–1269.
9. Levy AD, Remotti HE, Thompson WM, Sobin LH, Miettinen M. From the archives of the AFIP: gastrointestinal stromal tumors: radiologic features with pathologic correlation. Radiographics 2003; 23:283–304.

10. Joensuu H, Fletcher C, Dimitrijevic S, Silberman S, Roberts P, Demetri G. Management of malignant gastrointestinal stromal tumors. Lancet Oncol 2002; 3:655–664.
11. Emory TS, Sobin LH, Lukes L, Lee DH, O'Leary TJ. Prognosis of gastrointestinal smooth-muscle (stromal) tumors: dependence on anatomical site. Am J Surg Pathol 1999; 23:82–87.
12. Ozan E, Oztekin O, Alacacioğlu A, Aykaş A, Postaci H, Adibelli Z. Esophageal gastrointestinal stromal tumor with pulmonary and bone metastases. Diagn Interv Radiol 2010; 16:217–220.
13. Coleman RE. Clinical features of metastatic bone disease and risk of skeletal morbidity. Clin Cancer Res 2006; 12:6243–6249.
14. Mercadante S. Malignant bone pain: pathophysiology and treatment. Pain 1997; 69:1–18.
15. Petrut B, Trinkaus M, Simmons C, Clemons M. A primer of bone metastases management in breast cancer patients. Curr Oncol 2008; 15:50–57.